Scattering

M Mishchenko, L Travis, and A Lacis, Goddard Institute for Space Studies, New York, NY, USA

Synopsis

Sunlight illuminating the Earth's atmosphere is scattered by gas molecules and suspended particles, giving rise to blue skies, white clouds, and optical displays such as rainbows and halos. By scattering and absorbing the shortwave solar radiation and the longwave radiation emitted by the underlying surface, cloud and aerosol particles strongly affect the radiation budget of the terrestrial climate system. As a consequence of the dependence of scattering characteristics on particle size, morphology, and composition, scattered light can be remarkably rich in information on particle properties and thus provides a sensitive tool for remote retrievals of macro- and microphysical parameters of clouds and aerosols.

Introduction

A parallel beam of light, or of any electromagnetic radiation, propagates in a vacuum without a change in its characteristics. However, interposing a particle into the beam causes two fundamental effects. First, the particle may convert some of the energy contained in the electromagnetic field into other forms of energy such as heat. This phenomenon is called absorption. Second, the directional propagation of electromagnetic energy and its polarization state get modified. This phenomenon is called scattering.

The scattering and absorption characteristics of an isolated particle are often complex functions of the particle's size, morphology, and composition. They can be determined by obtaining a numerically exact solution of the Maxwell equations or by using a suitable experimental technique. Direct computer solutions of the Maxwell equations become much more involved and are often impracticable for a compound object in the form of a cloud of particles. In such cases, one has to use a physically based asymptotic solution of the Maxwell equations called the radiative transfer equation (RTE).

Sunlight incident on the Earth's atmosphere is scattered by gas molecules and suspended particles, giving rise to blue skies, white clouds, and various optical displays such as rainbows, halos, and the glory. By scattering and absorbing the shortwave solar radiation and the longwave radiation emitted by the underlying surface, cloud and aerosol particles strongly affect the radiation budget of the terrestrial climate system. As a consequence of the dependence of scattering characteristics on particle size, morphology, and composition, scattered light can be remarkably rich in implicit information on particle properties and thus provides a sensitive tool for remote retrievals of macro- and microphysical parameters of clouds and aerosols.

Electromagnetic Scattering by a Fixed Particle

To explain the fundamental concept of electromagnetic scattering by a fixed particle, let us assume that the electromagnetic field is time harmonic, which allows one to fully describe it at any moment in time everywhere in space as the solution of the frequency-domain Maxwell equations. Specifically, it is convenient to factor out the time-harmonic dependence of the complex electric and magnetic fields: $\mathbf{E}(\mathbf{r},t) = \exp(-\mathrm{i}\omega t)\,\mathbf{E}(\mathbf{r})$ and $\mathbf{H}(\mathbf{r},t) = \exp(-\mathrm{i}\omega t)\mathbf{H}(\mathbf{r})$, where $\mathbf{r}$ is the position vector of the observation point, t is time, ω is the angular frequency, and $\mathrm{i} = (-1)^{1/2}$. The actual electric and magnetic fields are obtained by taking the real part of the respective complex fields. The field amplitudes $\mathbf{E}(\mathbf{r})$ and $\mathbf{H}(\mathbf{r})$ can be found from the following curl equations:

$$\left.\begin{aligned}\nabla\times\mathbf{E}(\mathbf{r}) &= \mathrm{i}\omega\mu_0\,\mathbf{H}(\mathbf{r})\\ \nabla\times\mathbf{H}(\mathbf{r}) &= -\mathrm{i}\omega\varepsilon_1\mathbf{E}(\mathbf{r})\end{aligned}\right\}\text{inside } V_{\mathrm{EXT}}, \qquad [1]$$

$$\left.\begin{aligned}\nabla\times\mathbf{E}(\mathbf{r}) &= \mathrm{i}\omega\mu_0\,\mathbf{H}(\mathbf{r})\\ \nabla\times\mathbf{H}(\mathbf{r}) &= -\mathrm{i}\omega\varepsilon_2(\mathbf{r},\omega)\mathbf{E}(\mathbf{r})\end{aligned}\right\}\text{inside } V_{\mathrm{INT}}. \qquad [2]$$

Here, V_{INT} is the cumulative 'interior' volume occupied by the scattering particle; V_{EXT} is the infinite exterior region, which is assumed to be homogeneous, linear, isotropic, and nonabsorbing; the host medium and the particle are assumed to be nonmagnetic; μ_0 is the permeability of a vacuum; ε_1 is the real-valued electric permittivity of the host medium; and $\varepsilon_2(\mathbf{r},\omega)$ is the complex permittivity of the particle. Since the first relations in eqns [1] and [2] yield the magnetic field provided that the electric field is known everywhere, the solution of the Maxwell equations is usually sought in terms of only the electric field. To have a unique solution, eqns [1] and [2] must be supplemented by appropriate boundary conditions at the particle surface as well as by the so-called radiation conditions at infinity.

Note that although the amplitudes $\mathbf{E}(\mathbf{r})$ and $\mathbf{H}(\mathbf{r})$ do not depend on time explicitly, they can fluctuate randomly if the electromagnetic field is quasimonochromatic. However, such fluctuations are assumed to occur much more slowly than the time-harmonic oscillations described by the factor $\exp(-\mathrm{i}\omega t)$, which justifies the use of the frequency-domain Maxwell equations at any given moment.

Let us now assume that in the absence of the particle, the electromagnetic field is given by the simplest solution of the Maxwell equations in the form of a plane electromagnetic wave propagating in the direction of the wave vector $\mathbf{k}^{\mathrm{inc}}$:

$$\mathbf{E}^{\mathrm{inc}}(\mathbf{r}) = \mathbf{E}_0^{\mathrm{inc}}\exp\left(\mathrm{i}\mathbf{k}^{\mathrm{inc}}\cdot\mathbf{r}\right) \text{ everywhere in space.} \qquad [3]$$

As shown schematically in **Figure 1(a)**, eqn [3] represents the transport of electromagnetic energy from one point to another in the absence of the particle and embodies the concept of

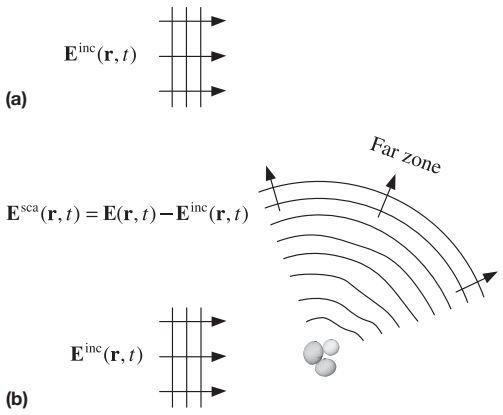

Figure 1 Electromagnetic scattering by a fixed particle. In this case, the particle is an aggregate consisting of three monomers in contact.

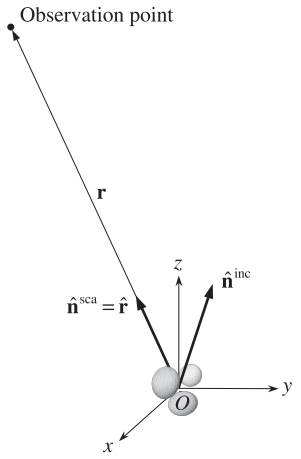

Figure 2 Scattering in the far zone of the particle.

a perfectly monochromatic parallel beam of light. The presence of the particle modifies the electromagnetic field that would exist otherwise. It is this modification that is called *electromagnetic scattering*.

It is customary to call the difference between the total field in the presence of the particle (i.e., $\mathbf{E}(\mathbf{r})$) and the original field that would exist in the absence of the object (i.e., $\mathbf{E}^{\text{inc}}(\mathbf{r})$) the 'scattered field' and denote it as $\mathbf{E}^{\text{sca}}(\mathbf{r})$ (see Figure 1(b)). Thus, the total field in the presence of the particle is intentionally represented as the sum of the respective incident (original) and scattered fields:

$$\mathbf{E}(\mathbf{r}) = \mathbf{E}^{\text{inc}}(\mathbf{r}) + \mathbf{E}^{\text{sca}}(\mathbf{r}). \quad [4]$$

Of course, one can think of incident fields other than a plane wave and thereby generalize the concept of scattering. In this regard, an especially convenient framework is provided by the so-called volume integral equation which follows from the Maxwell equations and incorporates the boundary and radiation conditions:

$$\mathbf{E}(\mathbf{r}) = \mathbf{E}^{\text{inc}}(\mathbf{r}) + k^2 \int_{V_{\text{INT}}} d\mathbf{r}' \overleftrightarrow{G}(\mathbf{r},\mathbf{r}') \cdot \mathbf{E}(\mathbf{r}') \left[m^2(\mathbf{r}') - 1 \right], \quad [5]$$

where $m(\mathbf{r}') = [\varepsilon_2(\mathbf{r}',\omega)/\varepsilon_1]^{1/2}$ is the refractive index of the interior relative to that of the host exterior medium; $k = |\mathbf{k}^{\text{inc}}| = \omega(\varepsilon_1\mu_0)^{1/2} = 2\pi/\lambda$ is the wave number; λ is the wavelength; $\overleftrightarrow{G}(\mathbf{r},\mathbf{r}')$ is the free-space dyadic Green's function; and $\mathbf{E}^{\text{inc}}(\mathbf{r})$ is any physically realizable solution of the Maxwell equations for an infinite homogeneous medium. One can see that eqn [5] expresses the total field everywhere in space in terms of the total internal field. The latter is not known in general and must be found by solving eqn [5] either analytically or numerically.

Far-Field Scattering

Equation [5] can be used to show that at a distance from the particle greatly exceeding its size, in the so-called far zone, the scattered field becomes an outgoing spherical wave (Figure 1(b)). By placing the origin O of the spherical coordinate system at the geometrical center of the particle (Figure 2), we have:

$$\mathbf{E}^{\text{sca}}(\mathbf{r}) \underset{r\to\infty}{\to} \frac{\exp(ikr)}{r} \mathbf{E}_1^{\text{sca}}(\hat{\mathbf{n}}^{\text{sca}}), \quad [6]$$

where $r = |\mathbf{r}|$ is the distance from the origin, $\hat{\mathbf{n}}^{\text{inc}} = \mathbf{k}^{\text{inc}}/k$ is a unit vector in the incidence direction, and $\hat{\mathbf{n}}^{\text{sca}} = \mathbf{r}/r$ is a unit vector in the scattering direction.

The electric and magnetic field vectors of the scattered spherical wave are perpendicular to the scattering direction, while those of the incident plane wave are normal to the incidence direction. It is therefore convenient to denote by $\mathbf{E}$ a two-element column formed by the θ- and φ-components of either electric field vector:

$$\mathbf{E} = \begin{bmatrix} E_\theta \\ E_\varphi \end{bmatrix}. \quad [7]$$

As usual, the polar (zenith) angle $0 \le \theta \le \pi$ is measured from the positive z-axis, while the azimuth angle $0 \le \varphi < \pi$ is measured from the positive x-axis in the clockwise direction when looking in the direction of the positive z-axis. The use of this notation allows us to write the scattered field as:

$$\mathbf{E}^{\text{sca}}(r\hat{\mathbf{n}}^{\text{sca}}) = \frac{\exp(ikr)}{r} \mathbf{S}(\hat{\mathbf{n}}^{\text{sca}}, \hat{\mathbf{n}}^{\text{inc}}) \mathbf{E}_0^{\text{inc}}, \quad [8]$$

where $\mathbf{S}$ is the 2×2 so-called amplitude scattering matrix expressing the θ- and φ-components of the scattered spherical wave in those of the incident plane wave. This relation plays a key role in the theory of electromagnetic scattering.

Optical Observables

The typically high frequency of time-harmonic electromagnetic oscillations makes it virtually impossible to measure the electric and magnetic fields associated with the incident and scattered waves using traditional optical instruments. Therefore, in order to make the theory applicable to analyses of actual observations, the scattering phenomenon must be characterized in terms of derivative quantities that can be measured directly (i.e., optical *observables*). The conventional approach to

address this problem is to use four real-valued quantities I, Q, U, and V, which have the dimension of monochromatic energy flux (Wm^{-2}) and fully characterize a transverse electromagnetic wave inasmuch as it is subject to practical optical analysis. These quantities, called the Stokes parameters, are always defined with respect to a plane containing the direction of wave propagation, form the four-element Stokes column vector $\mathbf{I}$, and carry information about both the total intensity I and the polarization state of the wave. The Stokes parameters are intentionally defined such that the rapidly oscillating time-harmonic factor $\exp(-\mathrm{i}\omega t)$ vanishes upon multiplication by its complex–conjugate counterpart: $\exp(-\mathrm{i}\omega t)[\exp(-\mathrm{i}\omega t)]^* \equiv 1$, where the asterisk denotes complex conjugation.

In the case of scattering in the far zone, both the incident plane wave and the outgoing scattered spherical wave are transverse. This allows one to define the corresponding sets of Stokes parameters:

$$\mathbf{I}^{\mathrm{inc}} = \begin{bmatrix} I^{\mathrm{inc}} \\ Q^{\mathrm{inc}} \\ U^{\mathrm{inc}} \\ V^{\mathrm{inc}} \end{bmatrix} = \frac{1}{2}\sqrt{\frac{\varepsilon_1}{\mu_0}} \begin{bmatrix} E_{0\theta}^{\mathrm{inc}}\left(E_{0\theta}^{\mathrm{inc}}\right)^* + E_{0\varphi}^{\mathrm{inc}}\left(E_{0\varphi}^{\mathrm{inc}}\right)^* \\ E_{0\theta}^{\mathrm{inc}}\left(E_{0\theta}^{\mathrm{inc}}\right)^* - E_{0\varphi}^{\mathrm{inc}}\left(E_{0\varphi}^{\mathrm{inc}}\right)^* \\ -E_{0\theta}^{\mathrm{inc}}\left(E_{0\varphi}^{\mathrm{inc}}\right)^* - E_{0\varphi}^{\mathrm{inc}}\left(E_{0\theta}^{\mathrm{inc}}\right)^* \\ \mathrm{i}\left[E_{0\varphi}^{\mathrm{inc}}\left(E_{0\theta}^{\mathrm{inc}}\right)^* - E_{0\theta}^{\mathrm{inc}}\left(E_{0\varphi}^{\mathrm{inc}}\right)^*\right] \end{bmatrix}, \quad [9]$$

$$\mathbf{I}^{\mathrm{sca}}(r\hat{\mathbf{n}}^{\mathrm{sca}}) = \begin{bmatrix} I^{\mathrm{sca}} \\ Q^{\mathrm{sca}} \\ U^{\mathrm{sca}} \\ V^{\mathrm{sca}} \end{bmatrix} = \frac{1}{r^2}\frac{1}{2}\sqrt{\frac{\varepsilon_1}{\mu_0}} \begin{bmatrix} E_{1\theta}^{\mathrm{sca}}\left(E_{1\theta}^{\mathrm{sca}}\right)^* + E_{1\varphi}^{\mathrm{sca}}\left(E_{1\varphi}^{\mathrm{sca}}\right)^* \\ E_{1\theta}^{\mathrm{sca}}\left(E_{1\theta}^{\mathrm{sca}}\right)^* - E_{1\varphi}^{\mathrm{sca}}\left(E_{1\varphi}^{\mathrm{sca}}\right)^* \\ -E_{1\theta}^{\mathrm{sca}}\left(E_{1\varphi}^{\mathrm{sca}}\right)^* - E_{1\varphi}^{\mathrm{sca}}\left(E_{1\theta}^{\mathrm{sca}}\right)^* \\ \mathrm{i}\left[E_{1\varphi}^{\mathrm{sca}}\left(E_{1\theta}^{\mathrm{sca}}\right)^* - E_{1\theta}^{\mathrm{sca}}\left(E_{1\varphi}^{\mathrm{sca}}\right)^*\right] \end{bmatrix}. \quad [10]$$

Then the responses of well-collimated polarization-sensitive radiometers located in the far zone of the particle can be described in terms of the 4×4 phase and extinction matrices as follows.

In the absence of the particle (Figure 3(a)), radiometer 2 registers no signal, whereas radiometer 1 reacts to the incident plane wave:

$$\textbf{Signal 1} = \Delta S \mathbf{I}^{\mathrm{inc}}, \quad [11]$$

$$\textbf{Signal 2} = \mathbf{0}, \quad [12]$$

where ΔS is the area of the objective lens. In the presence of the particle (Figure 3(b)), radiometer 2 reacts only to the scattered spherical wave, and its polarized reading is fully characterized by the product of the phase matrix $\mathbf{Z}$ and the Stokes column vector of the incident wave:

$$\textbf{Signal 2} = \Delta S \mathbf{I}^{\mathrm{sca}}(r\hat{\mathbf{n}}^{\mathrm{sca}}) = \frac{\Delta S}{r^2}\mathbf{Z}(\hat{\mathbf{n}}^{\mathrm{sca}}, \hat{\mathbf{n}}^{\mathrm{inc}})\mathbf{I}^{\mathrm{inc}}, \quad \hat{\mathbf{n}}^{\mathrm{sca}} \neq \hat{\mathbf{n}}^{\mathrm{inc}}. \quad [13]$$

The elements of the phase matrix have the dimension of area and are quadratic combinations of the elements of the amplitude scattering matrix $\mathbf{S}(\hat{\mathbf{n}}^{\mathrm{sca}}, \hat{\mathbf{n}}^{\mathrm{inc}})$. One can see that, in general, the phase matrix relates the Stokes parameters of the incident and scattered waves defined with respect to different reference planes: the meridional plane of the incidence direction $\hat{\mathbf{n}}^{\mathrm{inc}}$ and that of the scattering direction $\hat{\mathbf{n}}^{\mathrm{sca}}$, respectively.

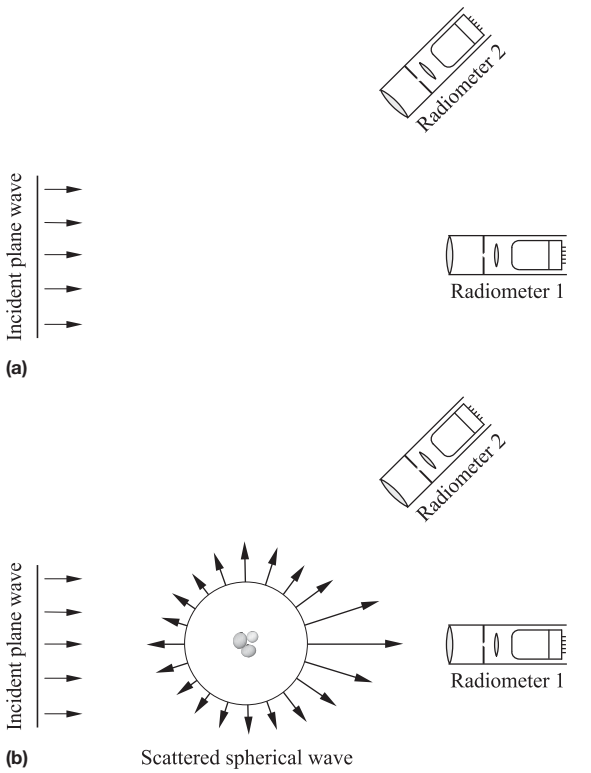

Figure 3 The readings of well-collimated polarization-sensitive radiometers in the presence of the particle differ from those in the absence of the particle.

Unlike radiometer 2, radiometer 1 in Figure 3(b) is facing the incident light, and, accordingly, its polarized reading consists of three parts:

1. the one due to the incident wave;
2. the one due to the forward-scattered wave; and
3. the one due to the interference of the incident wave and the wave scattered by the object in the exact forward direction:

$$\textbf{Signal 1} = \Delta S \mathbf{I}^{\mathrm{inc}} + \frac{\Delta S}{r^2}\mathbf{Z}(\hat{\mathbf{n}}^{\mathrm{inc}}, \hat{\mathbf{n}}^{\mathrm{inc}})\mathbf{I}^{\mathrm{inc}} - \mathbf{K}(\hat{\mathbf{n}}^{\mathrm{inc}})\mathbf{I}^{\mathrm{inc}}. \quad [14]$$

The third part is described by minus the product of the extinction matrix $\mathbf{K}$ and the Stokes column vector of the incident wave. The elements of the extinction matrix also have the dimension of area and are linear combinations of the elements of the forward-scattering amplitude matrix $\mathbf{S}(\hat{\mathbf{n}}^{\mathrm{inc}}, \hat{\mathbf{n}}^{\mathrm{inc}})$. Placing radiometer 1 sufficiently far from the particle makes the second term on the right-hand side of eqn [14] negligibly small.

In many respects, the measurement situation depicted in Figures 3(a) and 3(b) embodies the concept of electromagnetic scattering. Indeed, it demonstrates that in the absence of the particle, radiometer 2 would measure no signal, while the

signal measured by radiometer 1 allows one to measure the Stokes vector of the incident wave $\mathbf{I}^{\text{inc}}$. In the presence of the particle, the readings of both radiometers change. The reading of radiometer 2 is now proportional to the Stokes column vector of the scattered spherical wave, while the polarization signal measured by radiometer 1 is modified in two ways. First, the total measured electromagnetic power is attenuated as a combined result of the scattering of electromagnetic energy by the object in all directions and, possibly, the transformation of electromagnetic energy into other forms of energy (such as heat) inside the object. Second, the attenuation rates for the four Stokes components of the measured signal can, in general, be different. The latter effect is typical of objects lacking perfect spherical symmetry and is called dichroism.

Thus, to describe far-field scattering means, in effect, to quantify the differences between the readings of radiometers 1 and 2 in the presence of the object and in the absence of the object. This quantification can be fully achieved in terms of the phase and extinction matrices, which depend on object characteristics such as size, shape, refractive index, and orientation. Both matrices can be readily computed provided that the amplitude scattering matrix is already known.

In the case of quasimonochromatic fields, eqns [11]–[14] remain valid provided that now the Stokes column vectors of the incident and scattered fields are defined as averages of the right-hand sides of eqns [9] and [10] over a time interval much longer than the typical period of random fluctuations.

Derivative Quantities

There are several derivative quantities that are often used to describe various observable manifestations of electromagnetic scattering. The product of the extinction cross-section multiplied by the intensity of the incident plane wave yields the total attenuation of the electromagnetic power measured by radiometer 1 in Figure 3(b) owing to the presence of the particle. This means that the extinction cross-section depends, in general, on the polarization state and propagation direction of the incident wave and is given by:

$$C_{\text{ext}}(\hat{\mathbf{n}}^{\text{inc}}) = \frac{1}{I^{\text{inc}}}\left[K_{11}(\hat{\mathbf{n}}^{\text{inc}})I^{\text{inc}} + K_{12}(\hat{\mathbf{n}}^{\text{inc}})Q^{\text{inc}} + K_{13}(\hat{\mathbf{n}}^{\text{inc}})U^{\text{inc}} + K_{14}(\hat{\mathbf{n}}^{\text{inc}})V^{\text{inc}}\right]. \quad [15]$$

The product of the scattering cross-section multiplied by the intensity of the incident plane wave yields the total far-field power of the scattered wave:

$$C_{\text{sca}}(\hat{\mathbf{n}}^{\text{inc}}) = \frac{1}{I^{\text{inc}}}\int_{4\pi} d\hat{\mathbf{n}}^{\text{sca}}\left[Z_{11}(\hat{\mathbf{n}}^{\text{sca}}, \hat{\mathbf{n}}^{\text{inc}})I^{\text{inc}} + Z_{12}(\hat{\mathbf{n}}^{\text{sca}}, \hat{\mathbf{n}}^{\text{inc}})Q^{\text{inc}} + Z_{13}(\hat{\mathbf{n}}^{\text{sca}}, \hat{\mathbf{n}}^{\text{inc}})U^{\text{inc}} + Z_{14}(\hat{\mathbf{n}}^{\text{sca}}, \hat{\mathbf{n}}^{\text{inc}})V^{\text{inc}}\right]. \quad [16]$$

This implies that C_{sca} also depends on the polarization state as well as on the propagation direction of the incident wave. The absorption cross-section is defined as the difference between the extinction and scattering cross-sections:

$$C_{\text{abs}}(\hat{\mathbf{n}}^{\text{inc}}) = C_{\text{ext}}(\hat{\mathbf{n}}^{\text{inc}}) - C_{\text{sca}}(\hat{\mathbf{n}}^{\text{inc}}) \geq 0. \quad [17]$$

All optical cross-sections have the dimension of area. Finally, the dimensionless single-scattering albedo is defined as the ratio of the scattering and extinction cross-sections:

$$\tilde{\omega}(\hat{\mathbf{n}}^{\text{inc}}) = \frac{C_{\text{sca}}(\hat{\mathbf{n}}^{\text{inc}})}{C_{\text{ext}}(\hat{\mathbf{n}}^{\text{inc}})} \leq 1. \quad [18]$$

An important particular case of the phase matrix is the scattering matrix, defined by:

$$\mathbf{F}(\Theta) = \mathbf{Z}\left(\theta^{\text{sca}} = \Theta, \varphi^{\text{sca}} = 0;\ \theta^{\text{inc}} = 0, \varphi^{\text{inc}} = 0\right),\ 0 \leq \Theta < \pi, \quad [19]$$

where Θ, traditionally called the scattering angle, is the angle between the incidence and scattering directions. It is easy to see that the scattering matrix relates the Stokes parameters of the incident and scattered waves defined with respect to the same so-called scattering plane (i.e., the plane through the incidence and scattering directions).

Scattering by a Random Many-Particle Group

Although we have been so far discussing electromagnetic scattering by a 'single particle,' the concept of electromagnetic scattering and eqns [1]–[5] remain valid irrespective of the specific morphology of the scattering object. In particular, they are valid for what a human eye could classify as a 'collection of discrete particles.' Examples of such 'many-particle' objects are clouds, particulate surfaces, and particle suspensions. In all such cases, the electromagnetic field perceives a morphologically complex 'many-particle' object at any moment in time as one scatterer in the form of a specific spatial distribution of the relative refractive index throughout the cumulative interior volume V_{INT} in eqns [2] and [5].

However, the numerically exact computer solution of the Maxwell equations becomes prohibitively expensive when the size parameter of the object (i.e., the product of the wave number k and the radius of the smallest circumscribing sphere of the object) exceeds ~ 100. Furthermore, the concept of far-field scattering is inapplicable in the majority of practical situations involving very large many-particle groups such as clouds. Indeed, radiometers are often positioned inside or relatively close to the cloud (Figure 4) (i.e., in its near zone). As a consequence, one has to resort to an approximate computational technique and often abandon the attractively simple formulas of far-field scattering.

Two conventional approaches widely used to treat electromagnetic scattering by random particle groups are the single-scattering approximation (SSA) and the radiative transfer theory (RTT). The SSA is applicable to a relatively small, 'optically tenuous' group of N particles viewed from a distance much greater than the entire size of the group. In this case, eqns [11]–[14] remain valid provided that (1) the scattering signal is accumulated over a time interval long enough to establish full statistical randomness of the group; and (2) the phase, extinction, and scattering matrices of the entire group are also averaged over time. Then:

$$\left\langle \mathbf{Z}(\hat{\mathbf{n}}^{\text{sca}}, \hat{\mathbf{n}}^{\text{inc}})\right\rangle_t = N\left\langle \mathbf{Z}(\hat{\mathbf{n}}^{\text{sca}}, \hat{\mathbf{n}}^{\text{inc}})\right\rangle_\xi, \quad [20]$$

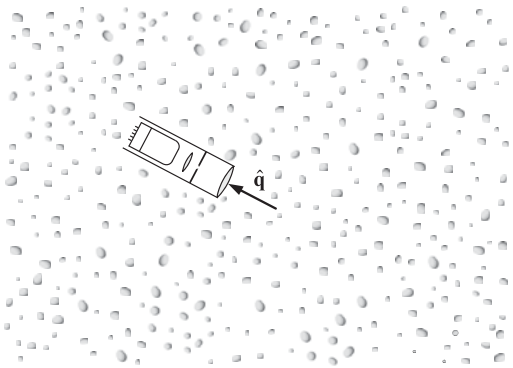

Figure 4 A well-collimated polarization-sensitive radiometer is placed inside a cloud of particles.

$$\langle \mathbf{K}(\hat{\mathbf{n}}^{\text{inc}}) \rangle_t = N \langle \mathbf{K}(\hat{\mathbf{n}}^{\text{inc}}) \rangle_\xi, \qquad [21]$$

$$\langle \mathbf{F}(\Theta) \rangle_t = N \langle \mathbf{F}(\Theta) \rangle_\xi, \qquad [22]$$

where $\langle \mathbf{Z}(\hat{\mathbf{n}}^{\text{sca}}, \hat{\mathbf{n}}^{\text{inc}}) \rangle_\xi$, $\langle \mathbf{K}(\hat{\mathbf{n}}^{\text{inc}}) \rangle_\xi$, and $\langle \mathbf{F}(\Theta) \rangle_\xi$ are the *single-particle* phase, extinction, and scattering matrix, respectively, averaged over all physically realizable particle states ξ in the group. The state of a particle indicates collectively its size, refractive index, shape, and orientation (i.e., all physical characteristics except the position). Note that it is the assumption of full ergodicity of the random scattering process that allows one to replace time averaging by ensemble averaging in eqns [20]–[22]. Obviously, the time averages of the extinction, scattering, and absorption cross-sections of the entire random particle group can be expressed similarly in terms of the respective ensemble-averaged single-particle cross-sections. The single-scattering albedo of the group is then given by:

$$\tilde{\omega}(\hat{\mathbf{n}}^{\text{inc}}) = \frac{\langle C_{\text{sca}}(\hat{\mathbf{n}}^{\text{inc}}) \rangle_\xi}{\langle C_{\text{ext}}(\hat{\mathbf{n}}^{\text{inc}}) \rangle_\xi}. \qquad [23]$$

The RTT is an expressly near-field theory that has recently been derived directly from the Maxwell equations and allows one to model the response of a well-collimated radiometer located inside or relatively close to a random multiparticle scattering object (Figure 4). Among the conditions of applicability of the RTE are the asymptotic requirement $N \to \infty$; the 'low-density' requirement, according to which every particle must be located sufficiently far from all the other particles; and the assumption that the scattering signal is accumulated over a time interval long enough to establish full ergodicity of the random scattering process. The integro-differential form of the RTE reads:

$$\hat{\mathbf{q}} \cdot \nabla \tilde{\mathbf{I}}(\mathbf{r}, \hat{\mathbf{q}}) = -n_0 \langle \mathbf{K}(\hat{\mathbf{q}}) \rangle_\xi \tilde{\mathbf{I}}(\mathbf{r}, \hat{\mathbf{q}}) + n_0 \int_{4\pi} d\hat{\mathbf{q}}' \langle \mathbf{Z}(\hat{\mathbf{q}}, \hat{\mathbf{q}}') \rangle_\xi \tilde{\mathbf{I}}(\mathbf{r}, \hat{\mathbf{q}}'), \qquad [24]$$

where n_0 is the average particle number density, $d\hat{\mathbf{q}}'$ is an elementary solid angle centered on the unit vector $\hat{\mathbf{q}}'$, and $\tilde{\mathbf{I}}(\mathbf{r}, \hat{\mathbf{q}})$ is the four-component so-called specific Stokes column vector. Unlike the Stokes column vectors [9] and [10], $\tilde{\mathbf{I}}(\mathbf{r}, \hat{\mathbf{q}})$ has the dimension of radiance ($\text{Wm}^{-2}\,\text{sr}^{-1}$). Thus, knowledge of the ensemble-averaged single-particle phase and extinction matrices is also required in order to solve the RTE.

The fundamental importance of the RTT is that its solution, $\tilde{\mathbf{I}}(\mathbf{r}, \hat{\mathbf{q}})$, directly quantifies the response of a well-collimated polarization-sensitive radiometer oriented along the unit vector $\hat{\mathbf{q}}$ at the observation point $\mathbf{r}$ (Figure 4). Furthermore, the integral $\int_{4\pi} d\hat{\mathbf{q}} \hat{\mathbf{q}} \tilde{I}(\mathbf{r}, \hat{\mathbf{q}})$ gives the time-averaged Poynting vector describing the direction and rate of the local electromagnetic energy transport. Thus, the RTT is directly applicable to solving both remote-sensing and radiation budget problems.

Symmetries

In general, all elements of the extinction and phase matrices entering eqns [13] and [14] can be nonzero, which implies that the intensity I registered by radiometers 1 and 2 in Figure 3(b) can depend on all four Stokes parameters of the incident field rather than only on its intensity. This fact emphasizes the vectorial (rather than scalar) character of electromagnetic scattering. In particular, dichroism results in different attenuation rates for different polarization components of the incident field. This causes, for example, depolarization of radar signals propagating through precipitation. The scattered wave recorded by radiometer 2 in Figure 3(b) also has polarization characteristics different from those of the incident field, thereby making polarimetry a sensitive particle characterization technique.

In many cases of practical interest, the mathematical structure of the ensemble-averaged extinction, phase, and scattering matrices becomes much simpler. This happens, for example, when (1) the distribution of particle orientations in a random group during the measurement is uniform, and (2) each particle in the group has a plane of symmetry and/or is accompanied by its mirror counterpart. Then the average extinction, scattering, and absorption cross-sections and the single-scattering albedo become independent of the direction of propagation and polarization state of the incident field. The average extinction matrix is diagonal and given by:

$$\langle \mathbf{K}(\hat{\mathbf{n}}^{\text{inc}}) \rangle_\xi \equiv \langle \mathbf{K} \rangle_\xi = \langle C_{\text{ext}} \rangle_\xi \, \text{diag}[1, 1, 1, 1]. \qquad [25]$$

The average phase matrix satisfies certain useful symmetry relations and depends on only the difference between the azimuthal angles of the scattering and incidence directions rather than on their specific values. The average scattering matrix has a simple block-diagonal structure with only six independent elements:

$$\langle \mathbf{F}(\Theta) \rangle_\xi = \begin{bmatrix} \langle F_{11}(\Theta) \rangle_\xi & \langle F_{12}(\Theta) \rangle_\xi & 0 & 0 \\ \langle F_{12}(\Theta) \rangle_\xi & \langle F_{22}(\Theta) \rangle_\xi & 0 & 0 \\ 0 & 0 & \langle F_{33}(\Theta) \rangle_\xi & \langle F_{34}(\Theta) \rangle_\xi \\ 0 & 0 & -\langle F_{34}(\Theta) \rangle_\xi & \langle F_{44}(\Theta) \rangle_\xi \end{bmatrix}. \qquad [26]$$

Furthermore,

$$\langle F_{12}(0) \rangle_\xi = \langle F_{12}(\pi) \rangle_\xi = 0, \quad \langle F_{34}(0) \rangle_\xi = \langle F_{34}(\pi) \rangle_\xi = 0. \qquad [27]$$

For spherically symmetric particles, the number of independent scattering matrix elements reduces to four owing to

the identities $\langle F_{22}(\Theta)\rangle_\xi \equiv \langle F_{11}(\Theta)\rangle_\xi$ and $\langle F_{44}(\Theta)\rangle_\xi \equiv \langle F_{33}(\Theta)\rangle_\xi$. As a consequence, measurements of the linear backscattering depolarization ratio

$$\delta_L = \frac{\langle F_{11}(\pi)\rangle_\xi - \langle F_{22}(\pi)\rangle_\xi}{\langle F_{11}(\pi)\rangle_\xi + \langle F_{22}(\pi)\rangle_\xi}, \quad 0 \le \delta_L \le 1 \qquad [28]$$

and the closely related circular backscattering depolarization ratio

$$\delta_C = \frac{\langle F_{11}(\pi)\rangle_\xi + \langle F_{44}(\pi)\rangle_\xi}{\langle F_{11}(\pi)\rangle_\xi - \langle F_{44}(\pi)\rangle_\xi} = \frac{2\delta_L}{1-\delta_L} \ge \delta_L \qquad [29]$$

are among the most reliable means of detecting particle nonsphericity.

Measurement and Computation of Single-Particle Characteristics

Evaluation of the Earth's radiation balance and analyses of remote-sensing observations require accurate quantitative knowledge of average single-particle optical characteristics as functions of particle size, morphology, and composition. This knowledge can be based on theoretical computations or experimental measurements, both approaches having their strengths and limitations. Theoretical modeling does not involve expensive instrumentation and allows switching to another particle shape, size, or refractive index by changing a few lines in a computer code. However, numerically exact computations for realistic polydispersions of morphologically complex particles are costly, if even possible, and are often replaced by computations for idealized shapes, whereas approximate calculations often have uncertain accuracy and range of applicability. Experimental measurements deal with real particles, but require complex and expensive hardware and may be difficult to interpret.

Measurements

Detectors of visible and infrared light are usually polarization insensitive, so their response is determined by only the first Stokes parameter of the incoming beam. In order to measure all elements of the scattering matrix, one must insert into the beam various optical elements that can vary the polarization state of light before and after scattering in a controllable way (Figure 5). The use of high-frequency sinusoidal modulation in the time of the polarization of light before scattering combined with intensity normalization and followed by lock-in detection increases the measurement accuracy and yields several elements from only one detected signal. The measurement procedure is repeated at different scattering angles in order to determine the angular profile of the scattering matrix.

Scattering measurements using visible and infrared light benefit from the availability of sensitive detectors (photomultipliers and avalanche semiconductor photodiodes), intense sources of radiation (lasers), and high-quality optical elements. They involve relatively inexpensive and portable instrumentation and can be performed in the field nearly as well as in the laboratory. However, they often suffer from poor advance knowledge of microphysical characteristics of scattering particles, thereby making difficult comparisons of experimental and theoretical results. The arrangement of the source of light and the detector precludes measurements at scattering angles close to 0° and 180°, which makes problematic the absolute measurement of the (1,1) element of the scattering matrix and the scattering cross-section.

The main idea of the microwave analog technique is to manufacture a centimeter-sized scattering object with desired shape and refractive index, measure the scattering of a microwave beam by this object, and finally extrapolate the results to other wavelengths (e.g., visible or infrared) by keeping the ratio of size and wavelength fixed. This allows one to determine so-called scale-invariant characteristics such as the phase

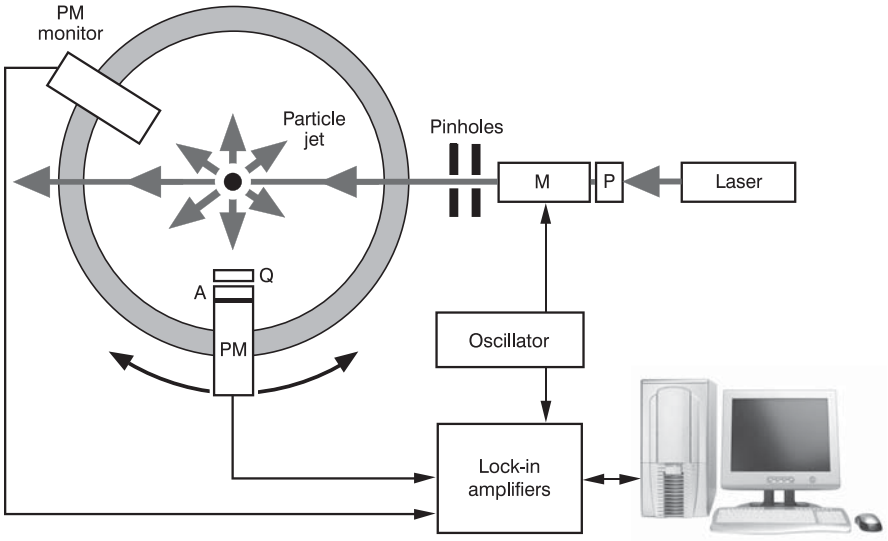

Figure 5 Schematic view of an experimental scattering setup using visible or infrared light. The laser beam passes several optical elements before and after scattering and is detected by the photomultiplier. The latter is mounted on a circular rail and can be moved around the particle jet in order to cover a wide range of scattering angles. A, polarization analyzer; M, electro-optic modulator; P, polarizer; PM, photomultiplier; Q, quarter-wave plate.

function $p(\Theta) = 4\pi\langle F_{11}(\Theta)\rangle_\xi / \langle C_{sca}\rangle_\xi$ or ratios of the elements of the scattering matrix. Microwave measurements allow a wide coverage of scattering angles, including the exact forward and backward directions, and a much greater degree of control over the target size, shape, and orientation than do optical measurements. However, the microwave measurements require more cumbersome and expensive instrumentation and large measurement facilities. Furthermore, they are performed for only one particle size, shape, and orientation at a time, thereby making ensemble averaging a time-consuming process.

Theoretical Techniques

All of the needs of a practitioner dealing with electromagnetic scattering by spherical particles may be well served by the exact and highly efficient Lorenz–Mie theory, which is the result of applying the separation-of-variables method to the Maxwell equations in spherical coordinates. There are extensions of the Lorenz–Mie theory applicable to concentric layered spheres.

For nonspherical particles, numerically exact computations must resort to more general and complex solutions traditionally divided into two broad categories. Differential equation methods compute the scattered field by solving the Maxwell equations, subject to appropriate boundary conditions, in the frequency domain or in the time domain. Integral equation methods are based on the volume or surface integral counterparts of the Maxwell equations; the boundary conditions are included in the solution automatically. Perhaps the most popular and widely used techniques are the *T*-matrix method, the discrete dipole approximation, and the finite-difference time-domain method. These techniques have somewhat different ranges of applicability in terms of particle morphology, refractive index, and size relative to the wavelength.

The practical importance of approximate treatments of light scattering diminishes as various exact techniques mature and become applicable to a wider range of problems, and as computers become ever more powerful. However, at least one phenomenological approach is unlikely to become obsolete in the near future because its accuracy can only be expected to improve as the ratio of the particle size to the wavelength grows, while numerically exact theoretical techniques for nonspherical particles cease to be practical whenever this ratio exceeds a certain threshold. This so-called geometrical optics approximation assumes that the particle size is much larger than the wavelength and that the incident plane wave can be represented as a collection of 'independent parallel rays.' The history of each ray impinging on the particle surface is traced using Snell's law and Fresnel formulas (**Figure 6**). Sampling all escaping rays into predefined narrow angular bins yields a quantitative representation of the particle scattering and absorption properties. The ray-tracing pattern is supplemented by computation of the Fraunhofer diffraction of the incident wave on the particle projection.

Solution of the RTE

Based on the specific problem at hand, the RTE [24] must be supplemented by appropriate boundary conditions. For example, a standard model of the atmosphere is a multilayer plane-parallel system illuminated from above by solar radiation and bounded from below by a horizontally homogeneous reflecting surface. Then the RTE can be solved numerically using efficient techniques such as the adding and doubling, discrete ordinate, and invariant imbedding methods. Complex horizontally and vertically inhomogeneous models can be handled using the less efficient but more flexible Monte Carlo technique.

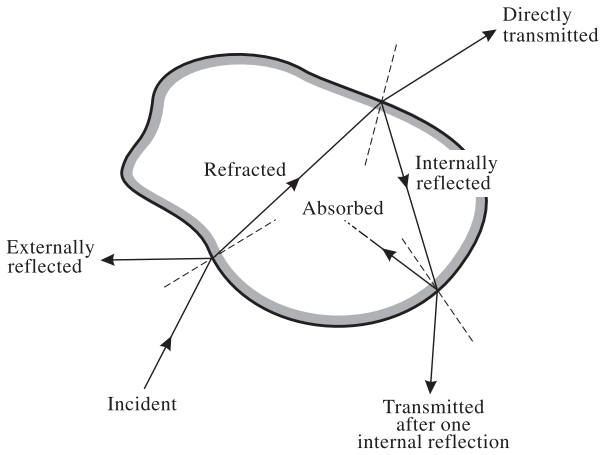

Figure 6 Ray-tracing diagram.

Despite the expressly vectorial nature of electromagnetic scattering, the RTE [24] is often replaced by a simplified scalar version in which one keeps only the first Stokes parameter (i.e., the intensity) and only the (1,1) elements of the extinction and phase matrices. Although it is much easier to solve the scalar RTE, it is important to remember that it has no physical justification and can result in significant errors in the computed intensity.

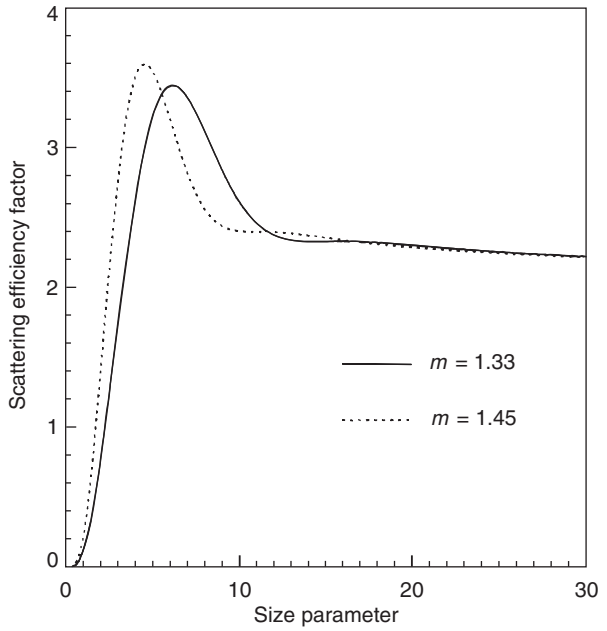

Figure 7 Scattering efficiency factor versus size parameter for polydisperse spherical particles with refractive indices 1.33 and 1.45.

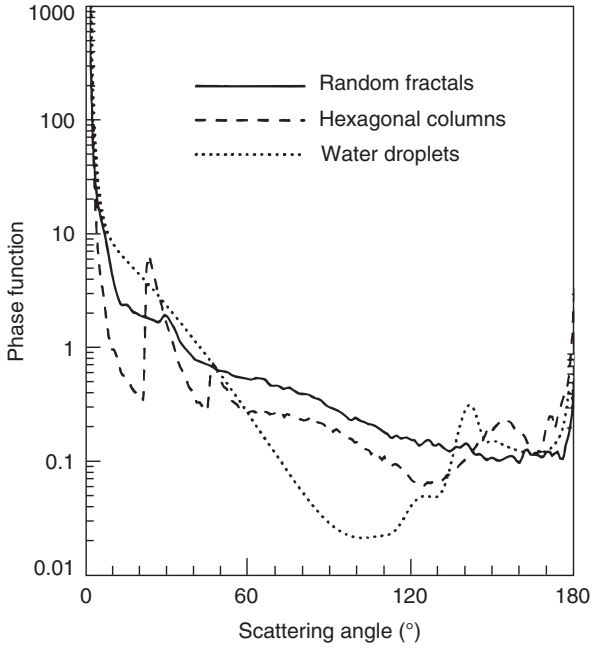

Figure 8 Phase functions for water cloud droplets, hexagonal ice columns, and randomly shaped ice crystals.

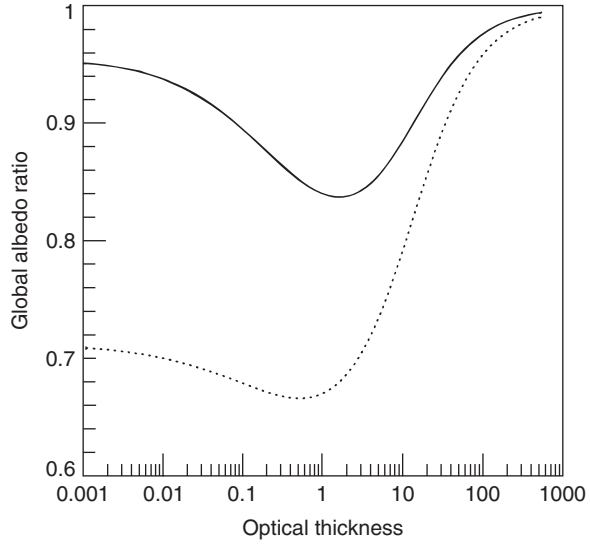

Figure 9 Global albedo of a liquid water cloud relative to that of an optical-thickness-equivalent ice cloud composed of irregular particles (dotted curve) and hexagonal columns (solid curve).

Examples of Scattering by Clouds and Aerosols

The few following examples serve to illustrate some key features of electromagnetic scattering phenomena and their use in remote sensing of aerosols and clouds and in radiation budget computations. Figure 7 shows the scattering efficiency factor Q_{sca} versus size parameter x for a narrow size distribution of spherical particles with refractive indices $m = 1.33$ and 1.45 (typical of water and sulfate aerosols at visible wavelengths,

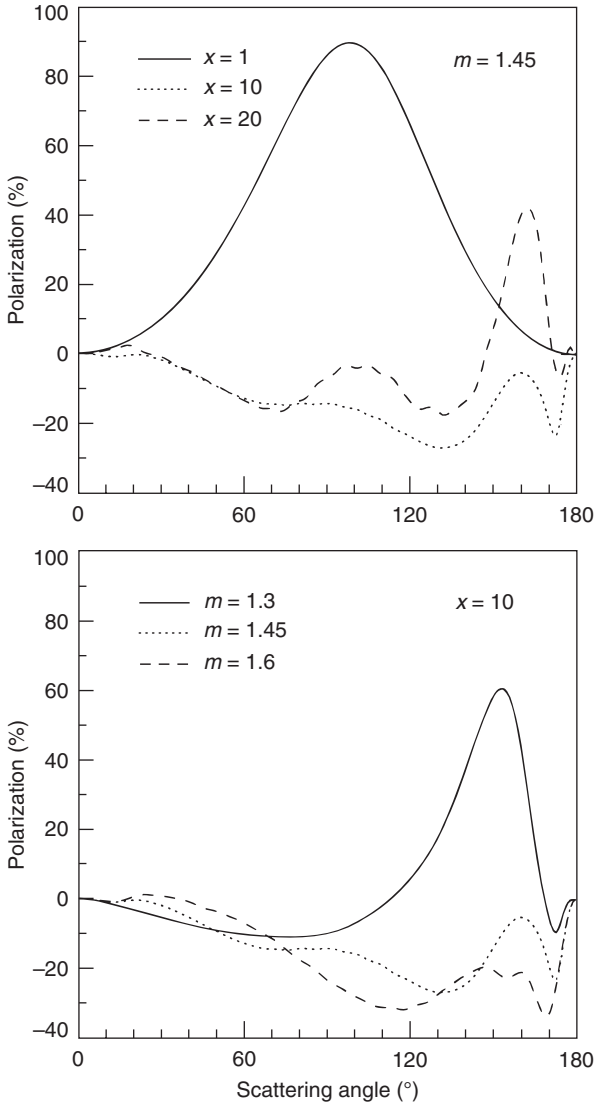

Figure 10 Linear polarization versus scattering angle for polydisperse spherical particles with varying size parameters x and refractive indices m.

respectively). The size parameter is defined as $x = 2\pi r_{eff}/\lambda$, where r_{eff} is the effective radius of the size distribution. The scattering efficiency is defined as the ratio of the average scattering cross-section to the average area of the particle geometrical projection. One can see that for wavelength-sized particles ($x \sim 5$), $\langle C_{sca}\rangle_{\xi}$ can exceed the particle geometrical cross-section by a factor greater than 3.5. As the particle size becomes much larger, Q_{sca} tends to the asymptotic geometrical-optics value of 2, with equal contributions from the rays striking the particle and the light diffracted by the particle projection. For particles much smaller than the wavelength, $Q_{sca} \propto \lambda^{-4}$, as first demonstrated by Lord Rayleigh and hence called Rayleigh scattering. The presence of a well-defined maximum in the scattering efficiency curve for a relatively narrow polydispersion (Figure 7) creates the possibility of an infrequent phenomenon for which aerosol particles of just the right size have a lower extinction efficiency factor in the blue than that at the larger wavelengths in the red. Thus, in contrast to the familiar

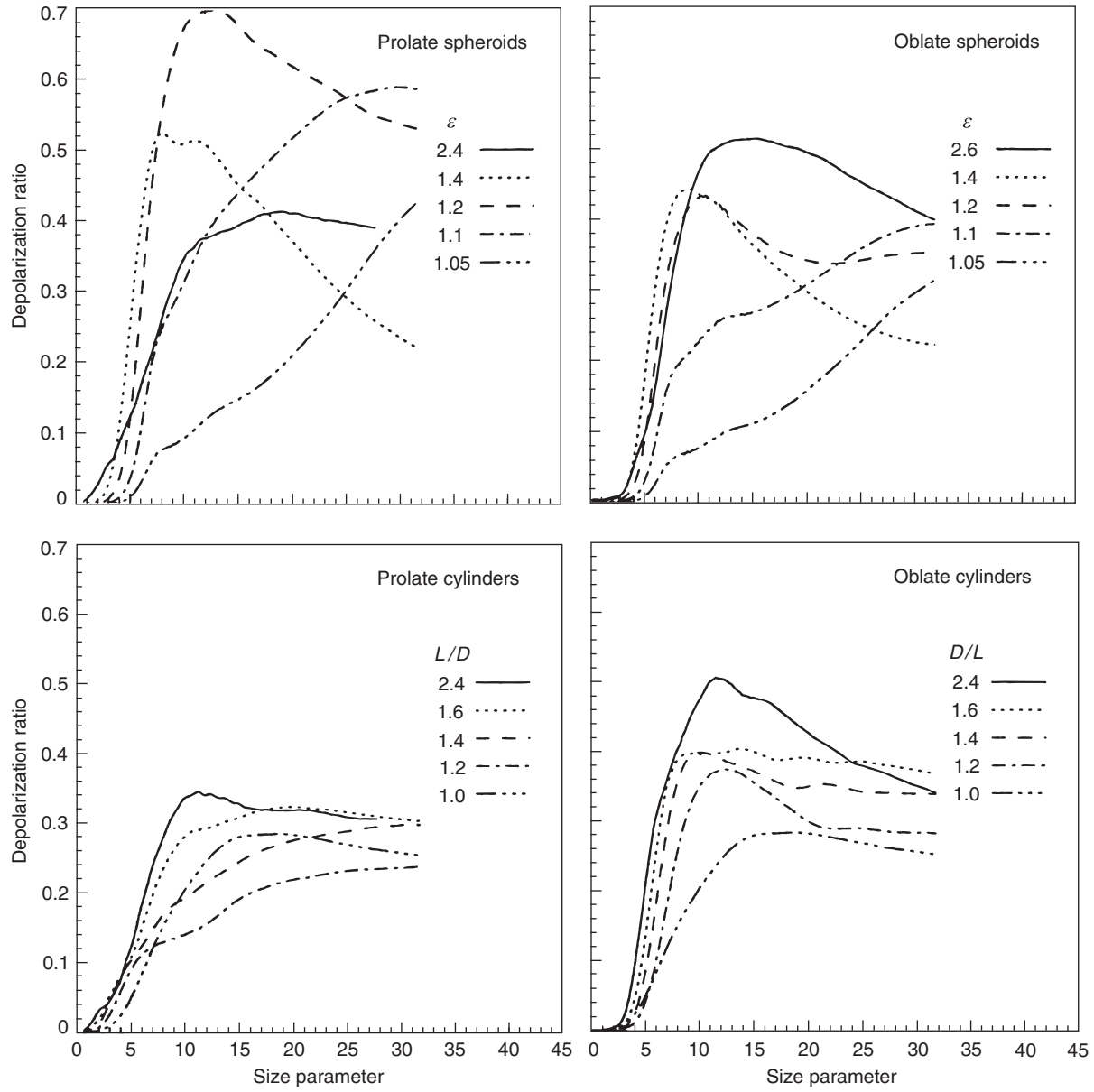

Figure 11 Linear depolarization ratio versus surface-equivalent sphere size parameter for polydisperse, randomly oriented ice spheroids and cylinders. The refractive index is 1.311. ε is the ratio of the largest to the smallest axes of a spheroid. The shapes of prolate and oblate cylinders are specified by length-to-diameter L/D and diameter-to-length D/L ratios, respectively.

reddening of the setting sun owing to enhanced Rayleigh scattering, a sufficiently narrow size distribution of aerosol particles in the atmosphere can produce a blue cast to the sun or moon and is perhaps responsible for the implied rarity associated with the phrase 'once in a blue moon.'

The dotted curve in Figure 8 shows the phase function typical of spherical cloud droplets at visible wavelengths. The strong concentration of light at $\Theta = 0^\circ$ is produced by Fraunhofer diffraction of light on the particle projection, whereas the feature at $\Theta \sim 140^\circ$ is the primary rainbow generated by rays that have undergone only one internal reflection (Figure 6). The slight change of the rainbow angle with wavelength caused by dispersion gives rise to spectacularly colorful rainbows often observed during showers illuminated by the sun at an altitude lower than about 40°. The enhanced intensity at $\Theta \sim 180^\circ$ is called the glory and can be seen from an airplane as a series of colored rings around the shadow cast by the airplane on the cloud top.

The dashed curve in Figure 8 depicts the phase function typical of randomly oriented pristine hexagonal ice crystals. The concentrations of light at $\Theta \sim 22^\circ$ and 46° are the primary and secondary halos attributed to minimum angles of deviation by 60° and 90° ice prisms. These features represent only two of many optical phenomena associated with regularly shaped ice crystals. Since cirrus clouds rather often fail to exhibit halos, the majority of real ice crystals appear to have

highly irregular shapes and rough rather than flat surfaces. Such particles are better characterized by featureless phase functions like the one shown in Figure 8 by the solid curve and computed for a random-fractal model of ice crystals.

Large numerical differences between the three phase functions depicted in Figure 8 can cause significant differences in bidirectional reflectance of optical-thickness-equivalent water and ice clouds (optical thickness is defined as the average extinction cross-section per particle times the column particle number concentration). This, in turn, may lead to significant errors in the retrieved cloud optical thickness if remote-sensing reflectance measurements are inverted using an incorrect particle model.

Figure 9 illustrates the effect of particle shape on the global cloud albedo (defined as cloud reflectance averaged over all incidence and reflection directions) at visible wavelengths. The quantity (1 – cloud albedo) determines how much solar energy is absorbed or transmitted by the atmosphere and is an important climatological parameter. It is seen that for the same optical thickness, clouds composed of irregular ice crystals have the largest albedo, whereas those composed of water droplets are the least reflective. This result can be explained by very large differences between the respective phase functions at side-scattering angles, which are well seen in Figure 8.

Figure 10 illustrates the ratio $P(\Theta) = -\langle F_{12}(\Theta)\rangle_\xi / \langle F_{11}(\Theta)\rangle_\xi$ of the scattering matrix elements (called the degree of linear polarization of the scattered light for unpolarized incident light) for polydisperse spheres with different refractive indices and size parameters. The obvious significant variability of polarization with m and r_{eff} (or λ) makes it a very sensitive indicator of the particle microphysical properties. Furthermore, since P is a ratio of two intensities, it can be measured to a much greater precision than intensity. These two factors explain the remarkable potential of photopolarimetry as a remote-sensing tool for aerosol and cloud particle characterization.

Finally, Figure 11 demonstrates the linear depolarization ratio [28] for polydisperse, randomly oriented, nonspherical ice particles. It is well seen that the growth of the size parameter from 0 to about 10 rapidly changes δ_{L} from zero to large values sometimes approaching the theoretical limit $\delta_{\text{L,max}} = 1$. This behavior of backscattering depolarization makes it useful for sizing aerosol, cloud, and precipitation particles by performing multiwavelength lidar and radar measurements. It is also obvious that although backscattering depolarization is a reliable indicator of the presence of nonspherical particles, its magnitude is not always a good measure of the degree of particle nonsphericity.

See also: **Aerosols:** Role in Radiative Transfer. **Clouds and Fog:** Classification of Clouds; Cloud Microphysics; Contrails. **Lidar:** Atmospheric Sounding Introduction. **Radar:** Precipitation Radar. **Satellites and Satellite Remote Sensing:** Aerosol Measurements.

Further Reading

Chandrasekhar, S., 1960. Radiative Transfer. Dover, New York.
Davis, A.B., Marshak, A., 2010. Solar radiation transport in the cloudy atmosphere: a 3D perspective on observations and climate impacts. Reports on Progress in Physics 73, 026801.
Goody, R.M., Yung, Y.L., 1989. Atmospheric Radiation. Oxford University Press, New York.
Hansen, J.E., Travis, L.D., 1974. Light scattering in planetary atmospheres. Space Science Reviews 16, 527–610.
Lenoble, J. (Ed.), 1985. Radiative Transfer in Scattering and Absorbing Atmospheres: Standard Computational Procedures. Deepak, Hampton, VA.
Liou, K.N., 2002. An Introduction to Atmospheric Radiation. Academic Press, San Diego, CA.
Mishchenko, M.I., 2011. Directional radiometry and radiative transfer: a new paradigm. Journal of Quantitative Spectroscopy and Radiative Transfer 112, 2079–2094.
Mishchenko, M.I., Hovenier, J.W., Travis, L.D. (Eds.), 2000. Light Scattering by Nonspherical Particles. Academic Press, San Diego, CA.
Mishchenko, M.I., Travis, L.D., Lacis, A.A., 2002. Scattering, Absorption, and Emission of Light by Small Particles. Cambridge University Press, Cambridge.
Mishchenko, M.I., Travis, L.D., Lacis, A.A., 2006. Multiple Scattering of Light by Particles. Cambridge University Press, Cambridge.
Stephens, G.L., 1994. Remote Sensing of the Lower Atmosphere. Oxford University Press, New York.
van de Hulst, H.C., 1957. Light Scattering by Small Particles. Wiley, New York.
Wendisch, M., Yang, P., 2012. Theory of Atmospheric Radiative Transfer. Wiley-VCH, Weinheim, Germany.